Title: Improving the magnetic heating by disaggregating nanoparticles.

Author names and affiliations:

F Arteaga-Cardona,[a,b]

K Rojas-Rojas,[a,b]

R Costo,[c]

MA Mendez-Rojas,[b]

A Hernando,[a,d]

P de la Presa[a,d,*]

[a] Instituto de Magnetismo Aplicado, UCM-ADIF-CSIC, A6 22,500 Km, 28230 Las Rozas, Spain

[b] Dto. Ciencias Químico-Biológicas, UDLAP, 72810 Puebla, Mexico

[c] Instituto de Ciencias de Materiales de Madrid, ICMM-CSIC, Sor Juana Inés de la Cruz, 3, Cantoblanco, 28049 Madrid, Spain

[d] Dto. Física Materiales, UCM, Ciudad Universitaria, 28040 Madrid, Spain

Corresponding author:

Patricia de la Presa

Instituto de Magnetismo Aplicado, UCM-ADIF-CSIC,

A6 22,500 Km, 28230 Las Rozas, Spain

pmpresa@ucm.es

Tel: +34 913 00 7173

Fax: +34 913 00 7176

Abstract. Recently, potential applications of the magnetic heating for heterogeneous catalysis or organic synthesis have been reported. As these new applications are not limited by biocompatibility requirements, a wide range of possibilities for non-aqueous colloidal nanoparticles with enhanced magnetic properties is open. In this work, manganese and cobalt ferrite nanoparticles are synthesized by co-precipitation method with average particle size around 12 nm. The particles are either coated with tetramethylammonium hydroxide (TMAOH) and dispersed in water or with oleic acid (OA) and dispersed in hexane to produce aggregated or disaggregated nanoparticles, respectively. It is observed that the particle disaggregation improves significantly the heating efficiency from 12 to 96 W/g in the case of cobalt ferrite, and from 120 to 413 W/g for the manganese ferrite. The main responsible for this improvement is the reduction of hydrodynamic volume that allows a faster Brownian relaxation. This work also discusses the relevance of the size distribution.

Keywords:

Magnetic heating, cobalt ferrite, manganese ferrite, nanoparticles, SAR, hyperthermia

1. Introduction

The heating efficiency of magnetic nanoparticle is nowadays intensively investigated because the applications to magnetic cancer therapy.[1-6] However, the potential applications for heterogeneous catalysis has been recently been reported.[7] Additionally, there is recent evidences that different chemical reactions in liquid media can be triggered using heating induced by iron oxide nanoparticles.[8] These new concepts consist in taking advantage of the heating efficiency of the nanoparticles under alternating magnetic field to produce in-situ catalysis or to induce organic synthesis. This opens a new and wide range of possibilities in the area of heating efficiency of nanoparticles. First of all, biocompatibility is no more a requirement, thus, any kind of metals or metal alloys (Fe, Co, Ni, FeCo, etc) or any magnetic oxide with enhanced magnetic properties can be used.[7, 9-13] Second, the dispersion media can be organic or inorganic; this provides different magnetic properties to the nanoparticles compared to the aqueous colloids.[9, 14] Finally, new frequency and amplitude field ranges can be explored because no limitation in the product $Hf < 5x10^9$ A/ms [see Ref. [15]] is necessary for a catalytic process.

At present, ferrite nanoparticles are the most common material for hyperthermia because the low toxicity, good magnetic properties and straightforward synthesis by ecofriendly routes, where the spinel structures can be obtained with high crystallinity degree. Thus, the heating efficiency in aqueous colloids of these materials is well established.[16-21]

It is know that for an assembly of interacting particles which are at the limit of superparamagnetic to ferromagnetic behavior, the role of dipolar interactions on the heating efficiency is to diminish the effective field acting on a particle, i.e., for isolated non-interacting particles, the heating is more effective than in the case of interacting particles.[22-27] At very low concentrations, the state of interacting or non-interacting particles depends on aggregation degree. Nanoparticles dispersed in water form aggregates, therefore, the particles are interacting independently of the concentration.[14, 16] On the other hand, particles synthesized in organic media are disaggregated and the interactions depend then on concentration; thus, the heating efficiency can be improved significantly by disaggregating the particles.[14]

In addition, the aggregation degree also plays a significant role for those particles whose heating mechanism is mainly given by Brownian relaxation. Specially, this is the case for the magnetic nanoparticles with high magnetic anisotropy, as the cobalt ferrite. In the case of aggregates, large hydrodynamic sizes slow down the Brownian relaxation diminishing the heating efficiency; the particles must be disaggregated in order to get faster relaxations. On the other hand, manganese ferrites are soft materials which main relaxation mechanism in given by Neel although Brownian relaxation cannot be discarded at all.

This work discusses the influence of aggregation degree and size distribution on the SAR for the case of cobalt and manganese ferrites. We show that the disaggregation of nanoparticles improves significantly the heating efficiency because the release of the Brownian relaxations.

2. Experimental Methods

2.1. Materials

Manganese (II) chloride tetrahydrate (99%) is purchased from Alfa Aesar. Iron (III) chloride hexahydrate (97%), cobalt (II) hexahydrate (98%), tetramethylammonium hydroxide solution (10%wt), hexane (95%), hydrochloric acid (37%) and oleic acid are purchased from Sigma Aldrich. Sodium hydroxide (analytical grade) is purchased from Merck. All reagents are used without further purification.

2.2. *Synthesis of $MnFe_2O_4$ and $CoFe_2O_4$*

To synthetize the MNPs, 2.5 mmol of $MCl_2 \cdot nH_2O$ (n=6 for M = Co and n=4 for M = Mn) is dissolved in 250 µL of HCl (37%) and 4 mL of water is added. On the other hand, 5 mmol of $FeCl_3 \cdot 6H_2O$ is dissolved in 10 ml of water. Both solutions are heated at 50 ^oC, mixed and added to a solution of 50 ml NaOH (3 M) at 100 ^oC. The stirring is adjusted to 600 rpm, and a black precipitate is formed immediately. The synthesis temperature is kept constant at 100 ^oC with different reaction times *t* at 15, 30 and 60 min, in order to get different particle sizes. The samples are called M-t, with M = Mn, Co and *t* = 15, 30, 60, indicating the corresponding ferrite and the reaction time of the synthesis. After that, the mixture is cooled down to room temperature and magnetically separated, washed several times with distilled water under sonication. Finally, the precipitate is dispersed in 0.1 M TMAOH.[28] All samples are fractioned by centrifugation in order to select the smallest particle sizes.[29-30]

2.3. *Oleic Acid Coating (OA)*

To reduce particle agglomeration and produce a non-polar stable ferrofluid, 3 ml of dispersed NPs are magnetically separated from the TMAOH solution and then mixed with 500 µL of OA and 2 mL of hexane under vigorous stirring during 10 minutes.[31]

2.4. Structural and colloidal characterization

X-ray diffraction (XRD) patterns are measured by a multipurpose PANalytical X´pert MPD with Cu-K_α source. The X-ray patterns are collected between 10^o and 70^o in 2θ. The average

crystallite size (D_{XRD}) is calculated using the Scherrer equation with the full-width-half-maximum (FWHM) of the (311) peak.

The size and shape of the particles are measured by transmission electron microscopy (TEM) using a JEOL-2000FXII at 200 kV, and a high-resolution transmission electron microscope (HRTEM) with XEDS detector JEOL JEM 3000F operated at 300 kV. The samples are prepared by diluting MNPs in ethanol, a droplet of diluted sample is placed on a carbon coated copper grid and the solvent is evaporated at room temperature. The mean particle size and distribution are evaluated by measuring more than 100 particles by means of Digital Micrograph™. Afterwards, data are fitted to a Gaussian distribution to obtain the mean particle size (d_{NP}) and standard deviation (σ). The polydispersity degree is calculated as σ/d_{NP}, and is considered to be representative of the homogeneity of the particle sizes. In addition, an elemental analysis by energy dispersive spectroscopy (EDS) is performed in each sample.

Colloidal properties are studied in a Zetasizer Nano S, from Malvern Instruments. Hydrodynamic sizes of the particles in suspension, d_h, are measured by Dynamic Light Scattering (DLS) with the samples dispersed in water and hexane. Each hydrodynamic value is the result of three different measurements at different dilutions to avoid errors coming from multiple scattering; the scattering index for the solvent of the colloid, water or hexane, is used. The d_h is measured by DLS in volume because the presence of some few large aggregates could overestimates d_h when are obtained from the intensity data.

The Fe concentration is measured with an Inductively Coupled Plasma Optical Emission Spectrometer (ICP-OES) Perkin Elmer Optima 2100 DV. For this purpose samples are digested with nitric acid to oxidize the organic coating and then, with hydrochloric acid to dissolve the particles.

2.5. Magnetic characterization

Static magnetic measurements are carried out on powder samples by means of a Quantum Design vibrating sample magnetometer. Magnetization curves are measured up to 5 T at 5 K and 300 K. Zero field-cooled and field-cooled curves (ZFC-FC) are obtained from 5 to 300 K at 100 Oe applied magnetic field.

Heating capacities of the MNPs are measured with a commercial system Magnetherm 1.5 (Nanotherics) with a close circuit of water maintained at 16 ^{o}C that cools the coils. Additionally, the samples are placed inside a Dewar to avoid heat loss by convection or conduction. The samples are characterized under radiofrequency field with 110 kHz and 200 Oe field frequency and amplitude, respectively.

The temperature of the colloids is measured with a fiberoptical thermometer and registered with a computer. Prior to turning the magnetic field on, the sample temperature is recorded for about 30 s in order to ensure thermal stability and to have a baseline for the calculation of SAR. As the field is turned on, the temperature rise is measured either during 300 s or up to 80 °C for aqueous colloids and 40 ºC for hexane colloids, well below the corresponding boiling temperatures 100 ºC and 69 ºC, respectively. By performing a linear fit of data (temperature versus time) in the initial time interval, the slope $\Delta T/\Delta t$ can be obtained. As the measurements are performed in non-adiabatic conditions, the curve slopes $\Delta T/\Delta t$ are fitted only in the first few seconds after turning the magnetic field on. The time range is selected such as the slope is maximum, typically during the first 30 s.[32] Previously to any measurement, a blank sample containing only water is measured under the same conditions to ensure that there is no heating transfer from the coils.

Since the Fe concentrations are in the range 1−10 wt %, the SAR values can be calculated as $SAR = (C_{liq}/c_{Fe})(\Delta T/\Delta t)$, where C_{liq} is the specific heat capacity of water (4.185 J/gK) or hexane (2.28 J/gK) and c_{Fe} is the Fe weight concentration in the colloid.[18] Then, the SAR values are obtained by fitting the experimental heating curves and normalizing to the iron mass (W/g_{Fe}).

3. Results and Discussion

3.1. Structure, morphology and colloidal properties

The formation/growth of ferrite nanoparticles can be rationalized according with the well-known mechanism associated to the co-precipitation method. Initially, appropriate stoichiometric amounts of hydroxylated Fe(III) and Mn(II) or Co(II) ions are formed under acidic pH (1 to 4-5) conditions and mixed at low temperatures to obtain an homogeneous mixture. The hydroxylated metal complexes are highly unstable in solution and after rapid addition into a basic solution (pH 9-11), they rapidly condense through a two-step associative process, forming an oxo bridge (oxolation mechanism), reaching the saturation concentration in the solution, generating nuclei that act as seeds for crystal growth.[33] Polydispersibility and crystallinity of growing nanoparticles depend on the temperature and the reaction time. Lower times yield smaller nanoparticles with low polydispersibility, while longer times produce larger nanoparticles and greater dispersibilities.

Under the experimental synthetic conditions, highly crystalline Mn and Co ferrite nanoparticles are obtained with sizes that may correspond to single crystals or small crystalline domains aggregates. According to XRD patterns, the characteristic diffraction patterns correspond to a spinel structure. The diffraction peaks are indexed with manganese ferrite spinel (PDF # 73-

1964) and cobalt ferrite spinel (PDF # 03-0864); see Supporting Information (SI) figure S1. The average crystalline sizes calculated by the Scherrer formula are 49 and 27 nm for Mn-60 and Co-60, respectively.

TEM images of Mn and Co-ferrites at different time reactions are shown in SI figure S2. The polydispersity degree observed in these images can be explained by the synthesis temperature. The diffusion coefficient of the ions in the solution is governed by temperature, i.e., at high temperature there is a higher ion diffusion resulting in a faster and more erratic nanoparticle growth and thus, in higher polydispersity.[17] A lower temperature would produce particles with low polydispersity degree; however, to obtain particles with high crystallinity degree and homogeneous cations distribution (the magnetic properties strongly depend on both) high temperature is required.[34] Some authors report that, for coprecipitation method, temperature higher than 80 ºC is needed to achieve cobalt and manganese ferrite with large crystallinity degree.[31, 35-36] Therefore, the reaction times and the temperatures for the synthesis must be chosen as a compromise to obtain the lowest polidispersity and the highest crystallinity degree.

The frequency of the particle sizes and the corresponding Gaussian distribution fits are shown in SI figure S3. As can be seen, the reaction times play a very different role in the synthesis of both ferrites. In the case of Mn-t, reducing the reaction time from 60 to 30 min reduces dramatically the average d_{NP}, from 43 to 11.7 nm (see table 1 and figure S3). Further reduction of the reaction time does not affect the particle size. Therefore, the chosen reaction time for Mn ferrite is 30 min, in order to get the smallest size with the largest crystallinity degree. In the case of Co-t, a reaction time of 60 min produces particle sizes of around 18.6 nm; by decreasing it to 30 min, the d_{NP} is reduced to 17.0 nm with a large polydispersity. Finally, a reaction time of 15 min gives place to particles with 12.7 nm mean size and a relative low polydispersity (0.2). Therefore, the reaction time for Co ferrite is 15 min because it is possible to produce the smallest particles with the lowest polydispersity. The final average size of both ferrites is around 12 nm. Figure 1 shows HRTEM images for Mn-30 and Co-15, the samples have a relative good crystallinity degree as can be observed.

Additionally, EDS analyses in manganese and cobalt ferrites show an average composition $Mn_{1.01(3)}Fe_{1.98(3)}O_4$ and $Co_{0.97(3)}Fe_{2.03(3)}O_4$, which, taking into account the experimental errors, fits pretty well to the nominal one.

Table 1: Experimental results on mean particle sizes obtained by TEM and XRD and hydrodynamic size in volume with TMAOH and OA particle coating as characterized by DLS. Polydispersity degree (standard deviation/mean size) is included in parentheses. [(a)] The hydrodynamic size distribution of Mn-30 in TMAOH shows two population distributions, one around 30 nm and the other, with a much smaller contribution, above 200 nm.

	Particle size d_{NP} (nm)		Hydrodynamic size d_h (nm)	
Sample	**Crystallite size (311) D_{XRD}**	**Particle size D_{TEM}**	**TMAOH**	**OA**
Co-60	27	18.6(0.2)		
Co-30		17.0(0.3)		
Co-15		12.7(0.3)	38(0.4)	15(0.4)
Mn-60	49	43(>0.5)		
Mn-30		11.7(0.3)	30(0.4)[(a)]	14(0.4)
Mn-15		11.3(0.3)		

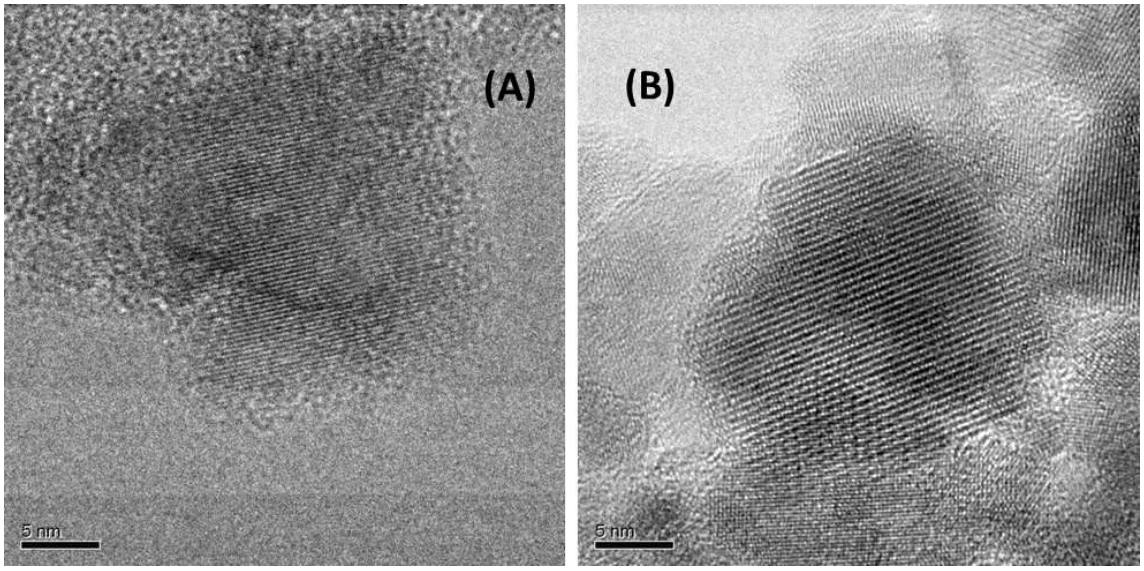

Figure 1. HRTEM images of (A) Mn-30 and (B) Co-15 (right) ferrites.

As expected, the hydrodynamic sizes are markedly different for particles coated with TMAOH and OA (see table 1 and figure. 2). DLS results show that TMAOH particles have larger hydrodynamic sizes than those with OA-coating. The hydrodynamic sizes for Co-15 can be reduced from 30 to 16 nm by coating the samples with OA instead TMAOH. On the other hand, the hydrodynamic size of the M-30 coated with TMAOH have a binomial volume distribution, one centered around 30 nm and the other, with a much smaller contribution, above 200 nm that can be reduced to 14 nm by OA coating (see Fig. 2).

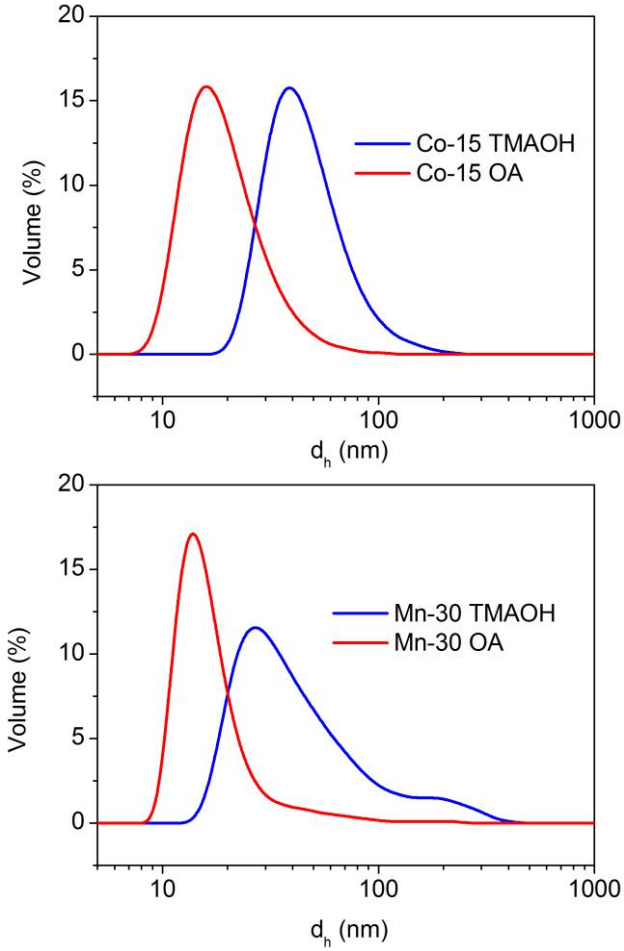

Figure 2. DLS in volume for Co-15 (upper panel) and Mn-30 (bottom panel) coated with TMAOH (blue line) and OA (red line).

It can be concluded that OA-coating disaggregates the Co and Mn ferrites nanoparticles leading to nearly individual particles stable in organic media (hexane). The table 1 summarizes the experimental results on particle sizes as well as the hydrodynamic sizes measured in water and hexane.

3.2. Magnetic properties

Spinel structure presents a face-centered cubic symmetry cell with 64 tetrahedral sites and 32 octahedral possible positions for cations, from which only 8 tetrahedral (A) sites and 16 octahedral [B] sites are occupied.[19] In particular, $CoFe_2O_4$ and $MnFe_2O_4$ in bulk present inverse spinel structures $(Fe)[MFe]O_4$ (M: Co, Mn), where () and [] mean A and B sites, respectively. At the nanometric scale, due to the large contribution of surface atoms, these ferrites present a mixed-spinel structure $(Fe_{1-x}M_x)[Fe_{1+x}M_{1-x}]O_4$ ($0 < x < 1$), where *x* is the inversion degree that indicates the cation distribution in the spinel structure.[37] It is known that inversion degree of

ferrites strongly affects their magnetic properties. Commonly, the exchange integrals J_{AB}, J_{BB}, J_{AA} are negative and the antiferromagnetic *A*–*B* interaction is stronger that the *A*–*A* and *B*–*B* interactions; therefore, ferrimagnetism arises from the decompensation of the magnetic moments in the *A* and *B* sublattices.

The field and thermal dependence of the magnetization provide information about the magnetic properties of these ferrites nanoparticles (see figures 3 and 4). As can be seen from table 2, the saturation magnetizations M_s values of Co-15 and Mn-30 are 77% and 72% of the corresponding bulk values.[38] Since for very small particles the proportion of coupled moment carriers is lower than in larger particles due to the high surface/volume ratio, it follows that the small particles have a lower net magnetization than the bulk samples. This can be thought as a kind of dead layer at the nanoparticle surface that decreases the net magnetization at T = 5 K in a factor $M_s / M_s^{bulk} \approx 0.75$, thus, the magnetic volume of the particle is smaller than the particle volume and the dead layer thickness can be estimated to be around 10% of the particle size.

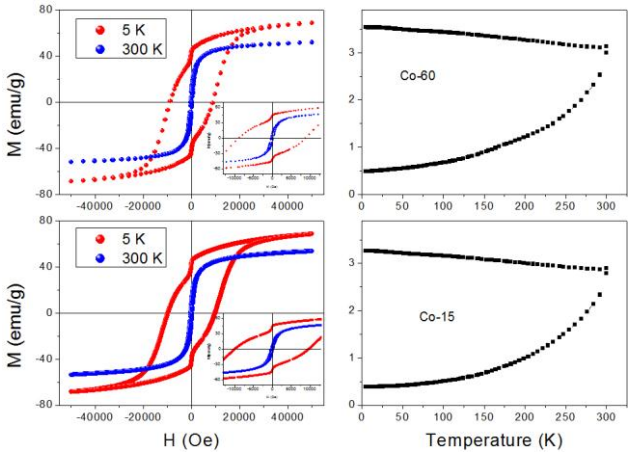

Figure 3. Magnetization loops (left panel) and ZFCFC curves (right panel) of samples Co-15 (bottom) and Co-60 (top).

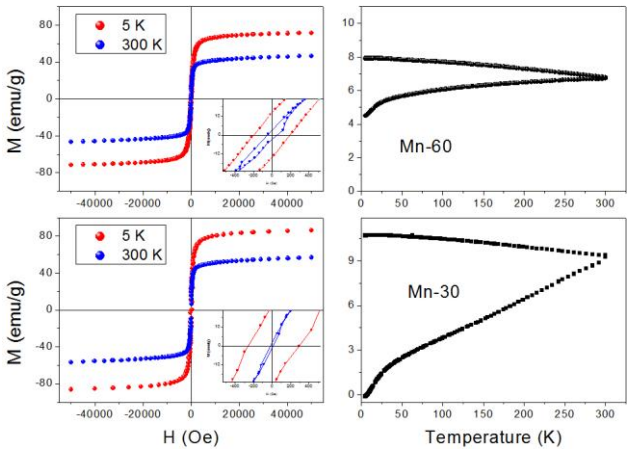

Figure 4: Magnetization loops (left panel) and ZFCFC curves (right panel) of samples Mn-30 (bottom) and Mn-60 (top).

Table 2: Saturation magnetization (M_s), coercive fields (H_c) and effective anisotropy (K_a) for manganese and cobalt ferrites. The bulk values are included for comparison.

Sample	M_s (emu/g)		H_c (Oe)		K_a (erg/cm^3)
	5 K	300 K	5 K	300 K	5 K
Co-60	68	52	8600	260	
Co-15	68	53	9800	277	$1.6\text{x}10^6$
Bulk	90	80			$4.4\text{x}10^6$
Mn-60	72	47	206	50	
Mn-30	86	57	260	<10	$0.1\text{x}10^6$
Bulk	120	80			$0.2\text{x}10^6$

As shown in Table 2, the coercive field increases as particle size decreases for Co-t nanoparticles. In the case of Mn-60 and Mn-30, similar behavior is observed at 5 K, i.e. the coercive field increases with decreasing particle size. However, at 300 K, the magnetization curve shows an almost superparamagnetic behavior, with a negligible coercive field for the smallest particles Mn-30 whereas the largest Mn-60 nanoparticles show a ferromagnetic behavior with a small coercive field. The observation of coercivity at RT for Co-t and Mn-60 indicates that the magnetic moments are blocked whereas Mn-30 is superparamagnetic.

The different coercivity values at 5 K among the samples can be ascribed to the strong dependence of coercive field to structural properties like particle size, particle size distribution, surface atoms, crystallinity degree, etc.[13] At 5 K, the rise of coercivity with the decreasing particle size could be related to the interactions between the surface layers formed by canted spins.[39-40] These interactions seem to modify the surface anisotropy, leading to an increase of the effective anisotropy K_{eff}. As it is known, the coercivity decrease with temperature is due to thermal energy that favors the particle moment reversal.

The full convergence of the ZFC and FC for Co-t curves just at RT (see fig. 3) indicates that the magnetic moments are blocked even at high temperature, confirming the results observed by the hysteresis loops. The critical size for superparamagnetism at RT in cobalt ferrites can be estimated from the equation $K_a V_c = 25 k_B T_B$, with k_B the Boltzman constant, T_B the blocking temperature, K_a the magnetic anisotropy of bulk, and V_c the critical volume. On the other hand, the effective anisotropy K_{eff} of the samples can be estimated form the anisotropy field $\mu_0 H_K = 2K_{eff} / M_s$, with M_s the saturation magnetization. $\mu_0 H_K$ can be obtained from the coercive field at 5 K as $\mu_0 H_K \simeq \mu_0 H_c(5\text{ K})$ since $\mu_0 H_c(T) = \mu_0 H_K(1 - T/T_B)$ and $T_B \geq 300\text{ K}$ for both ferrites. By considering the measured values H_c and M_s at 5 K, the

effective magnetic anisotropy is K_{eff} = 1.6x10^6 erg/cm^3, smaller than K_a = 4.4x10^6 erg/cm^3 for bulk cobalt ferrite at low temperature.[38] The critical volume for observation of superparamagnetism at RT is calculated to be around 8 nm. Therefore, no superparamagnetic behavior is expected for the 12.7 nm Co-ferrite nanoparticles even when K_{eff} is used for the calculation of the critical volume.

On the other hand, the magnetization of the Mn-t shows a different thermal behavior (see figure 4). The ZFC-FC curves of Mn-60 indicate that blocking temperature is well above RT whereas Mn-30 seems to be at the limit of superparamagnetic to ferromagnetic regimen. The calculated value K_{eff} = 0.1x10^6 erg/cm^3 by means of H_c at 5 K is comparable to the bulk value K_a ~ 0.2 10^6 erg/cm^3 (see Ref. [38]). The superparamagnetic behavior takes place only for particle sizes below ~20 nm. However, the average particle sizes for Mn-30 is around 12 nm with a relative high polydispersity degree. Thus, the thermal dependence of the magnetization reflects the contribution of the largest particles, which are the limit of superparamagnetic to ferromagnetic behavior.

3.3. Nanoparticle heating efficiency

For the following discussion we distinguish three different average particle volume: *i)* the magnetic volume $V_M = \frac{\pi}{6}\left(d_M\right)^3$, estimated from the reduced M_s values at 5 K (previous section), *ii)* the particle volume $V_{NP} = \frac{\pi}{6}\left(d_{NP}\right)^3$, measured by TEM, and *iii)* the hydrodynamic volume $V_h = \frac{\pi}{6}\left(d_h\right)^3$, measured by DLS. The different particle sizes obey the following relationship: $d_M < d_{NP} < d_h$.

Magnetic hyperthermia relies on the ability of the nanoparticles to convert the work of the magnetic field into thermal energy. The magnetic moment of a particle suspended in a fluid can relax after magnetic field removal by two different mechanisms described by $\tau_N = \tau_0 \exp\frac{K_{eff}V_M}{k_BT}$ and $\tau_B = \frac{3\eta V_h}{k_BT}$, the Neel and Brown relaxations, respectively,[41-42] where τ_0 is a length of time of the material usually between 10^{-9} to 10^{-11} s, K_{eff} is the anisotropy constant of the material, T is the temperature, η is the fluid viscosity and k_B is the Boltzmann constant.

The heating efficiency of magnetic nanoparticles is quantified by the SAR which, under the linear response theory (LRT), is expressed as $SAR \propto H_0\left[\left(2\pi f\right)^2 \tau_R \Big/ \left(1+\left(2\pi f \tau_R\right)^2\right)\right]$, where H_0 is the applied field, τ_R the relaxation time of the magnetic moments and f the measuring frequency.[43] The LRT is valid under the condition $\mu_0 M_s V_M H_0 < k_B T$; thus, for a given H_0 and T, the maximum d_M for which the LRT can be applied is determined by $\boldsymbol{M}_s$. Taking the M_s values from table 2 and considering the applied field amplitude 200 Oe (20 mT), the LRT is valid only for those nanoparticles with d_M smaller than 11.5 and 11.2 nm for Co-15 and Mn-30, respectively. These values are close to the average d_{NP} of each ferrite (see table 1) and, as previously discussed, $d_M < d_{NP}$ because of the presence of a dead layer at the nanoparticle surface.

Figure 5 shows the distribution of d_{NP} for Co-15 and Mn-30 and the validity range of the LRT which is calculated for V_{NP} (black solid line). Actually, the LRT is limited by the V_M (black dot line) that cannot be measured but roughly estimated from the loss of *Ms*. As we are dealing with distribution of particle sizes, it follows that the heating mechanism of part of the particles obeys the LRT whereas the rest does not.

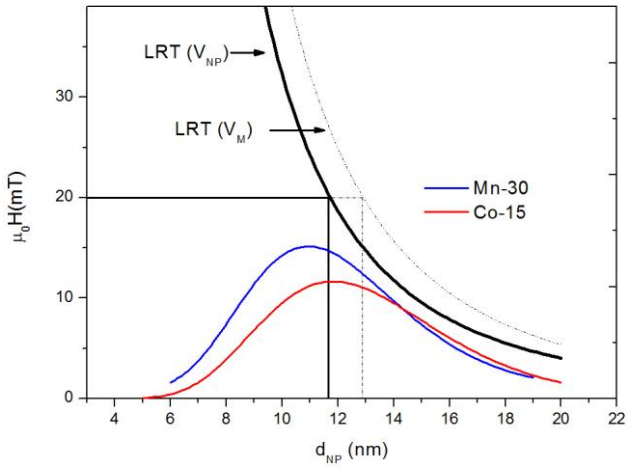

Figure 5: Maximum values of $\mu_0 H_0$ as a function of size for validity range of the LRT: $\mu_0 M_s V H_0 < k_B T$ (black solid curve). The blue and red solid line represents the particle size distribution for Mn-30 and Co-15, respectively. For $\mu_0 H_0 = 20$ mT (horizontal line) the maximum particle size is d_{NP} = 11.7 nm (vertical line), the magnetic response of those particles with d_{NP} >11.7 nm cannot be modeled by the LRT. If V_M instead V_{NP} is considered for the LRT validity range (black dotted curve); then, the limiting particle size shifts to larger sizes (vertical dotted line).

The heating mechanism of most of the particle can be described by the LRT if V_M instead V_{NP} is considered for the validity range of LRT. For the sake of simplicity, let us assume the LRT is valid for the whole particle sizes. For a given frequency, the maximum power loss is reached at $2\pi f \tau_R = 1$, which determines the relaxation time regarding the measuring frequency for the maximum heating efficiency; longer or shorter relaxation times lead to a SAR decrease. For the working frequency 110 kHz, the characteristic relaxation times τ_R is 1.4×10^{-6} s. Let´s define a time window $\Delta\tau_R$ such as those magnetic moments with relaxation times within the interval $0.4 < 2\pi f \tau_R < 2.6$ give SAR values which are at least two third of the maximum SAR.[44] We assume that, all the magnetic moments with τ_R within this time window, $\tau_R \subset \Delta\tau_R$, can contribute significantly to the heating.

The Neel relaxation is determined by K_{eff} and V_M; whereas the Brownian motion is governed by η and V_h. The large volume of the aggregates slows down the Brownian relaxation of the magnetic moments diminishing the heating efficiency; in order to shorten the relaxation time and get faster relaxations, V_h must be reduced. To achieve this, the cobalt and manganese ferrites are coated with OA and dispersed in hexane; OA has a high affinity to iron oxide and can stabilize the nanoparticles by steric repulsions.[45] Recently, maghemite nanoparticles produced by co-precipitation method have been successfully disaggregated by coating the particles with OA and dispersed them in hexane, resulting in an increase of the heating efficiency.[14]

The temperature increases as a function of time for cobalt and manganese ferrites are shown in figure 6. As can be seen, all the samples are able to heat, even the cobalt ferrites nanoparticles dispersed in water. The small temperature increase observed in the Co-60 and Co-15 nanoparticles coated with TMOAH and dispersed in water (figure 6A) can be unquestionably ascribed to the heating capacity of the sample when it is compared to the blank sample. The fitting of the heating curves (described in the experimental method) gives the SAR values shown in figure 7 and table 3. As can be seen, the OA coating improves the heating efficiencies in most of the cases with the exception of sample Mn-60, probably due to the large size of the particles (D_{XRD} > 40 nm).

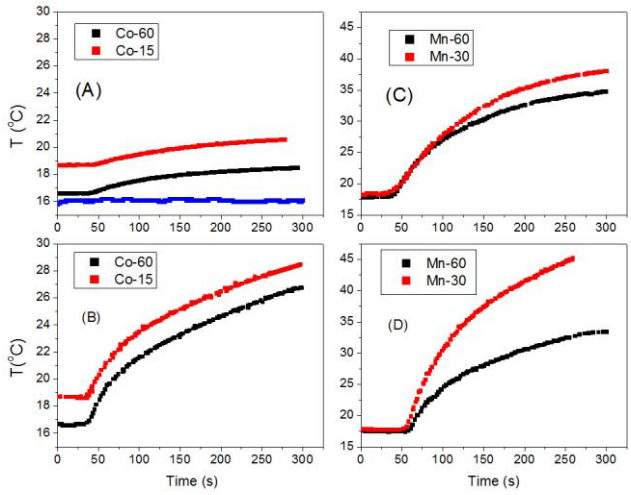

Figure 6: Heating curve at 110 kHz and 200 Oe of samples Co-60, Co-15, Mn-60 and Mn-30 with TMAOH dispersed in water (A, C) and coated with OA and dispersed with hexane (BD). The result for blank sample with pure water is shown in (A) with blue points.

Table 3: Iron concentration of the colloids, calculated Brownian relaxation times τ_B, SAR and ILP values at 110 kHz and 200 Oe for the TMAOH- and OA-coated Co-15 and Mn-30. The characteristic relaxation time at this frequency is $\tau_R = 1.4 \times 10^{-6}$ s.

	TMAOH				OA			
	C_{Fe} (mg_{Fe}/ml)	**τ_B** (μs)	**SAR** (W/g)	**ILP** (nHm^2/kg)	**C_{Fe}** (mg_{Fe}/ml)	**τ_B** (μs)	**SAR** (W/g)	**ILP** (nHm^2/kg)
Co-15	6	20.0	12	0.43	3	0.3	96	3.46
Mn-30	5	10.4	120	4.33	2	0.2	413	14.90

According to the ZFC-FC measurements, the Co-15 nanoparticles are blocked at RT; therefore, the main relaxation mechanism is due to Brownian movement of the aggregates.[16] The τ_B can be calculated from d_h (see table 3). When comparing both relaxation times, it is observed that the mean τ_B value for the particles with TMAOH in water is about 10 times longer than τ_R, whereas it becomes about 5 times shorter for the particles coated with OA in hexane. This reveals that, at this frequency, the relaxation of magnetic moments is too slow for the aggregated particles (particles in TMAOH) and too fast for the OA-coated particles to produce the maximum heating efficiency. However, the significant improvement of SAR for the disaggregated OA-coated ferrites, despite the too short τ_B, could be originated by the distribution of the hydrodynamic sizes (see figure 9). In size dispersed systems there exists a distribution of relaxation times because their volume dependence.[46]

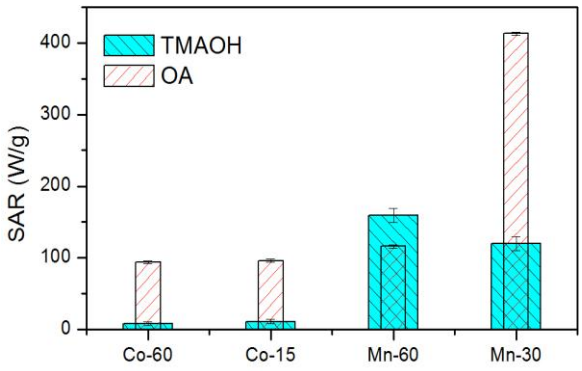

Figure 7: SAR values for Co and Mn ferrites coated with TMAOH and dispersed in water, and coated with OA and dispersed in hexane.

As in Co-15 the magnetic relaxations are given mainly by Brownian motion of the aggregates, then τ_R can be estimated with $\tau_R = \tau_B = \frac{3\eta V_h}{k_B T}$ by considering the aggregate sizes and the different viscosity of water (1 cP) and hexane (0.2 cP). Figure 8 shows the calculated τ_B and the frequency of the hydrodynamic sizes for water and hexane, figure 8(A) and (B), respectively. The selected time window $\Delta\tau_R$, for which SAR values are at least two third of the maximum, is indicated with two horizontal lines. As can be inferred from figure 8, in the case of Co-15 coated with TMOAH and dispersed in water, τ_R for each hydrodynamic size is virtually much longer than the upper limit of $\Delta\tau_R$, denoting that the magnetic relaxations are too slow to contribute to the heating. In the case of Co-15 coated with OA and dispersed in hexane, the relaxation is too fast for those aggregate sizes which are smaller than the average hydrodynamic size. However, in this case, there exists a significant contribution to the heating due to the large aggregates. Those particle sizes with $\tau_R \subset \Delta\tau_R$ are indicated by the shadow area of the size distribution. As can be seen, the number of aggregates that can contribute to the heating increases significantly in the case of OA coating regarding to TMOAH.

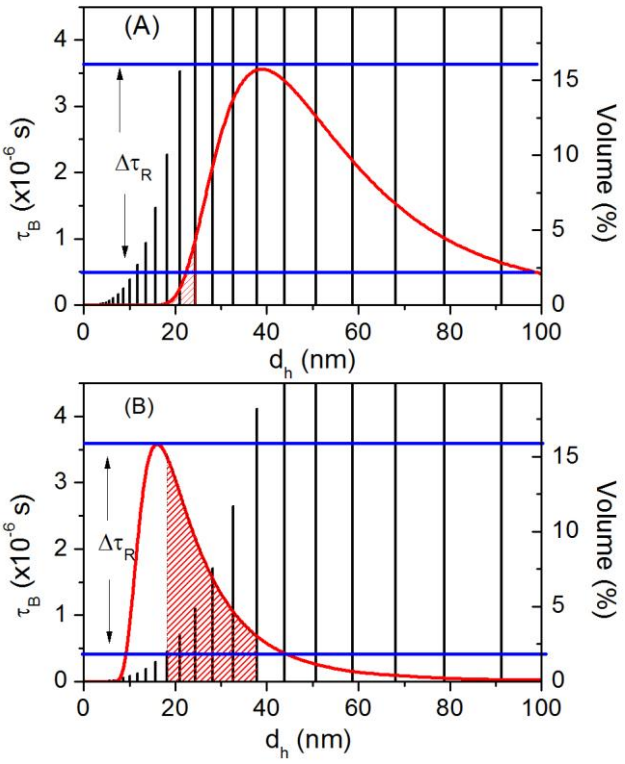

Figure 8: Hydrodynamic size distribution (red curve, right axis), calculated Brownian relaxation times τ_B (vertical bars, left axis) and time window $\Delta\tau_R$ (limited by the two horizontal lines) for A) Co-15 coated with TMAOH and dispersed in water, and B) Co-15 coated with OA and dispersed in hexane. The characteristic relaxation time at this frequency is τ_R = 1.4x10^{-6} s; the time window $\Delta\tau_R$ is chosen such as the relaxation times within the range $0.4 < 2\pi f \tau_R < 2.6$ lead to at least two third of the maximum SAR value. The shadows areas indicate the fraction of particle volume with $\tau_R \subset \Delta\tau_R$.

It is worth to noting that the LRT can be valid for hydrodynamic sizes d_h as large as those shown in figure 8 because the validity of the LRT is given by the magnetic size $d_M << d_h$.

For the Mn-30 particles, this analysis is more complicated because magnetization is at the limit from superparamagnetic to ferromagnetic behavior, and, thus, both relaxation mechanism, Neel and Brown, are present. The presence of both kind of mechanisms cause a relaxation given by $\frac{1}{\tau_R} = \frac{1}{\tau_N} + \frac{1}{\tau_B}$, where τ_N depends exponentially on V_M whereas τ_B depends linearly with V_h. However, there exists also a significant enhancement of the SAR when the particles are coated with OA, from 120 to 413 W/g, confirming the assumption that both relaxation mechanisms are present in manganese ferrites. The low magnetic anisotropy of manganese ferrite makes it a promising material as heating source because Neel and Brown relaxations can contribute to the

heating. Recently, a SAR value around 1600 W/g has been reported in $Mn_{0.5}Fe_{2.5}O_4$ around 20 nm in size.

The release of the Brownian motion is not the only responsible for the heating increase in the OA coated nanoparticles. It has been recently shown that 13 nm Fe_2O_3 particles, which are at the limit from superparamagnetic to ferromagnetic behavior, can improve significantly the heating efficiency with decreasing concentration when coated with OA and dispersed in hexane regarding the same particles dispersed in water.[14] This effect is mainly due to the lacking of dipolar interactions for disaggregated particles at low concentrations maximizes the effective field acting on the particle enhancing thus the heating efficiency.[23] As the particles coated with OA and TMOAH are produced in the same batch, i.e, they have the same magnetic and structural properties, and SAR measurements are performed at very low concentration, the cancelation of the particle interactions seems to contribute also to the improvement of the heating efficiency in OA- coated particles.

Another possible mechanism that can enhance the SAR is the particle chain formation.[27] However, the formation of chains requires of magnetic fields high enough to saturate low magnetic anisotropy nanoparticles. In this work we are working with magnetic fields within the validity range of the LRT, i.e, well below the saturation. Although the formation of chains cannot be discarded, the applied field is too low for such effect to be considered.

Unlike SAR, an intrinsic loss power (ILP) defined as $ILP = SAR/fH_0^2$ allows the comparison of the particle intrinsic properties.[47] This definition requires that the imaginary component of the magnetic susceptibility, $\chi''(t)$, is frequency independent in the range of frequency measurements and that the SAR characterization satisfies the condition of the LRT. Assuming that the previous conditions are valid in our system, we find an ILP value of 4.33 nHm^2/kg for Mn-30 in TMAOH, as can be seen in table 3, which makes this material very suitable for hyperthermia application because most of the ILP values for commercial ferrofluids are reported to be in the range 0.2 to 3.1 nHm^2/kg. In the case of OA-coated nanoparticles, they have still larger ILP values, which make them suitable for technological applications like in-situ heterogeneous catalysis or chemical reactions in liquid media.[7-8]

4. Conclusions

Manganese and cobalt ferrite nanoparticles synthesized by co-precipitation method with 12 nm average particle size, can be either coated with TMAOH or OA to form aqueous or organic colloids, respectively. The aqueous colloids form aggregates with high polidispersity, whereas

OA-coating disaggregates the nanoparticles and led to near individual particles with hydrodynamic sizes determined by the particle size plus the organic chain. The magnetic properties show that the cobalt ferrites are blocked at RT whereas manganese ferrites are at the limit from superparamagnetic to ferromagnetic behavior. It is observed that the particle disaggregation improves significantly the heating efficiency from 12 to 96 W/g in the case of cobalt ferrite, from 120 to 413 W/g for the manganese ferrite when measured under an alternating magnetic field of 110 kHz and 200 Oe. The particle disaggregation reduces the hydrodynamic volume allowing a faster Brownian relaxation; however, there exist other mechanisms, like cancellation of dipolar interactions or the formation of particle chains, which can contribute significantly to the enhancement of the particle heating efficiency.

These results show that manganese and cobalt ferrites can be promising materials for catalysis processes activated by heating magnetic nanoparticles under an alternating magnetic field.

Acknowledgments

This work was supported by grants from the Spanish Ministry of Science and Innovation (MAT2012-37109-C02-01), and Fundación Mutua Madrileña (Spain).

REFERENCES

1. Maier-Hauff, K.; Ulrich, F.; Nestler, D.; Niehoff, H.; Wust, P.; Thiesen, B.; Orawa, H.; Budach, V.; Jordan, A., Efficacy and safety of intratumoral thermotherapy using magnetic iron-oxide nanoparticles combined with external beam radiotherapy on patients with recurrent glioblastoma multiforme. J. Neuro-Oncol. 103 (2011) 317-324.
2. Johannsen, M.; Thiesen, B.; Wust, P.; Jordan, A., Magnetic nanoparticle hyperthermia for prostate cancer. Int. J. Hyperthermia 26 (2010) 790-795.
3. Kolosnjaj-Tabi, J.; Di Corato, R.; Lartigue, L.; Marangon, I.; Guardia, P.; Silva, A. K. A.; Luciani, N.; Clement, O.; Flaud, P.; Singh, J. V.; Decuzzi, P.; Pellegrino, T.; Wilhelm, C.; Gazeau, F., Heat-Generating Iron Oxide Nanocubes: Subtle "Destructurators" of the Tumoral Microenvironment. ACS Nano 8 (2014) 4268-4283.
4. Villanueva, A.; de la Presa, P.; Alonso, J. M.; Rueda, T.; Martinez, A.; Crespo, P.; Morales, M. P.; Gonzalez-Fernandez, M. A.; Valdes, J.; Rivero, G., Hyperthermia HeLa Cell Treatment with Silica-Coated Manganese Oxide Nanoparticles. J. Phys. Chem. C 114 (2010) 1976-1981.
5. Hervault, A.; Thanh, N. n. T. K., Magnetic nanoparticle-based therapeutic agents for thermo-chemotherapy treatment of cancer. Nanoscale 6 (2014) 11553-11573.
6. Silvio, D.; Rudolf, H., Magnetic particle hyperthermia—a promising tumour therapy? Nanotechnology 25 (2014) 452001.
7. Meffre, A.; Mehdaoui, B.; Connord, V.; Carrey, J.; Fazzini, P. F.; Lachaize, S.; Respaud, M.; Chaudret, B., Complex Nano-objects Displaying Both Magnetic and Catalytic Properties: A Proof of Concept for Magnetically Induced Heterogeneous Catalysis. Nano Letters 15 (2015) 3241-3248.

8. Kirschning, A.; Kupracz, L.; Hartwig, J., New Synthetic Opportunities in Miniaturized Flow Reactors with Inductive Heating. Chemistry Letters 41 (2012) 562-570.
9. Andreu, I.; Natividad, E.; Ravagli, C.; Castro, M.; Baldi, G., Heating ability of cobalt ferrite nanoparticles showing dynamic and interaction effects. Rsc Advances 4 (2014) 28968-28977.
10. Torres, T. E.; Roca, A. G.; Morales, M. P.; Ibarra, A.; Marquina, C.; Ibarra, M. R.; Goya, G. F., Magnetic properties and energy absorption of CoFe(2)O(4) nanoparticles for magnetic hyperthermia. International Conference on Magnetism (Icm 2009) 200 (2010) 4.
11. Lacroix, L. M.; Malaki, R. B.; Carrey, J.; Lachaize, S.; Respaud, M.; Goya, G. F.; Chaudret, B., Magnetic hyperthermia in single-domain monodisperse FeCo nanoparticles: Evidences for Stoner-Wohlfarth behavior and large losses. J. Appl. Phys. 105 (2009) 4.
12. Hyeon, T., Chemical synthesis of magnetic nanoparticles. Chemical Communications (2003) 927-934.
13. Blanco-Gutierrez, V.; Virumbrales, M.; Saez-Puche, R.; Torralvo-Fernandez, M. J., Superparamagnetic Behavior of MFe2O4 Nanoparticles and MFe2O4/SiO2 Composites (M: Co, Ni). The Journal of Physical Chemistry C 117 (2013) 20927-20935.
14. de la Presa, P.; Luengo, Y.; Velasco, V.; Morales, M. P.; Iglesias, M.; Veintemillas-Verdaguer, S.; Crespo, P.; Hernando, A., Particle Interactions in Liquid Magnetic Colloids by Zero Field Cooled Measurements: Effects on Heating Efficiency. The Journal of Physical Chemistry C 119 (2015) 11022-11030.
15. Hergt, R.; Dutz, S., Magnetic particle hyperthermia-biophysical limitations of a visionary tumour therapy. Journal of Magnetism and Magnetic Materials 311 (2007) 187-192.
16. de la Presa, P.; Luengo, Y.; Multigner, M.; Costo, R.; Morales, M. P.; Rivero, G.; Hernando, A., Study of Heating Efficiency as a Function of Concentration, Size, and Applied Field in γ-Fe2O3 Nanoparticles. The Journal of Physical Chemistry C 116 (2012) 25602−25610.
17. Salas, G.; Costo, R.; Morales, M. d. P., Chapter 2 - Synthesis of Inorganic Nanoparticles. In Frontiers of Nanoscience, Jesus, M. d. l. F.; Grazu, V., Eds. Elsevier: (2012)Vol. Volume 4, pp 35-79.
18. Gonzalez-Fernandez, M. A.; Torres, T. E.; Andres-Verges, M.; Costo, R.; de la Presa, P.; Serna, C. J.; Morales, M. R.; Marquina, C.; Ibarra, M. R.; Goya, G. F., Magnetic nanoparticles for power absorption: Optimizing size, shape and magnetic properties. Journal of Solid State Chemistry 182 (2009) 2779-2784.
19. Sharifi, I.; Shokrollahi, H.; Amiri, S., Ferrite-based magnetic nanofluids used in hyperthermia applications. Journal of Magnetism and Magnetic Materials 324 (2012) 903-915.
20. Mazario, E.; Sánchez-Marcos, J.; Menéndez, N.; Cañete, M.; Mayoral, A.; Rivera-Fernández, S.; de la Fuente, J. M.; Herrasti, P., High Specific Absorption Rate and Transverse Relaxivity Effects in Manganese Ferrite Nanoparticles Obtained by an Electrochemical Route. The Journal of Physical Chemistry C 119 (2015) 6828-6834.
21. Lemine, O. M.; Omri, K.; Iglesias, M.; Velasco, V.; Crespo, P.; de la Presa, P.; El Mir, L.; Bouzid, H.; Yousif, A.; Al-Hajry, A., γ-Fe2O3 by sol–gel with large nanoparticles size for magnetic hyperthermia application. Journal of Alloys and Compounds 607 (2014) 125-131.
22. Serantes, D.; Baldomir, D.; Martinez-Boubeta, C.; Simeonidis, K.; Angelakeris, M.; Natividad, E.; Castro, M.; Mediano, A.; Chen, D.-X.; Sanchez, A.; Balcells, L.; Martínez, B., Influence of dipolar interactions on hyperthermia properties of ferromagnetic particles. J. Appl. Phys. 108 (2010) 073918.
23. Haase, C.; Nowak, U., Role of dipole-dipole interactions for hyperthermia heating of magnetic nanoparticle ensembles. Physical Review B 85 (2012) 045435.
24. Piñeiro-Redondo, Y.; Bañobre-López, M.; Pardiñas-Blanco, I.; Goya, G.; López-Quintela, M.; Rivas, J., The influence of colloidal parameters on the specific power absorption of PAA-coated magnetite nanoparticles. Nanoscale Res Lett 6 (2011) 1-7.
25. Martinez-Boubeta, C.; Simeonidis, K.; Serantes, D.; Conde-Leborán, I.; Kazakis, I.; Stefanou, G.; Peña, L.; Galceran, R.; Balcells, L.; Monty, C.; Baldomir, D.; Mitrakas, M.;

Angelakeris, M., Adjustable Hyperthermia Response of Self-Assembled Ferromagnetic Fe-MgO Core–Shell Nanoparticles by Tuning Dipole–Dipole Interactions. Adv. Funct. Mater. 22 (2012) 3737-3744.
26. Mehdaoui, B.; Meffre, A.; Carrey, J.; Lachaize, S.; Lacroix, L. M.; Gougeon, M.; Chaudret, B.; Respaud, M., Optimal Size of Nanoparticles for Magnetic Hyperthermia: A Combined Theoretical and Experimental Study. Adv. Funct. Mater. 21 (2011) 4573-4581.
27. Mehdaoui, B.; Tan, R. P.; Meffre, A.; Carrey, J.; Lachaize, S.; Chaudret, B.; Respaud, M., Increase of magnetic hyperthermia efficiency due to dipolar interactions in low-anisotropy magnetic nanoparticles: Theoretical and experimental results. Physical Review B 87 (2013) 174419.
28. Pereira, C.; Pereira, A. M.; Fernandes, C.; Rocha, M.; Mendes, R.; Fernández-García, M. P.; Guedes, A.; Tavares, P. B.; Grenèche, J.-M.; Araújo, J. P.; Freire, C., Superparamagnetic MFe2O4 (M = Fe, Co, Mn) Nanoparticles: Tuning the Particle Size and Magnetic Properties through a Novel One-Step Coprecipitation Route. Chemistry of Materials 24 (2012) 1496-1504.
29. Tartaj, P.; Morales, M. d. P.; Veintemillas-Verdaguer, S.; González-Carreño, T.; Serna, C., The preparation of magnetic nanoparticles for applications in biomedicine. Journal of Physics D: Applied Physics 36 (2003) R182.
30. Gyergyek, S.; Drofenik, M.; Makovec, D., Oleic-acid-coated CoFe2O4 nanoparticles synthesized by co-precipitation and hydrothermal synthesis. Materials Chemistry and Physics 133 (2012) 515-522.
31. Auzans, E.; Zins, D.; Blums, E.; Massart, R., Synthesis and properties of Mn-Zn ferrite ferrofluids. Journal of Materials Science 34 (1999) 1253-1260.
32. Natividad, E.; Castro, M.; Mediano, A., Adiabatic vs. non-adiabatic determination of specific absorption rate of ferrofluids. Journal of Magnetism and Magnetic Materials 321 (2009) 1497-1500.
33. Thanh, N. T. K.; Maclean, N.; Mahiddine, S., Mechanisms of Nucleation and Growth of Nanoparticles in Solution. Chemical Reviews 114 (2014) 7610-7630.
34. Chen, J. P.; Sorensen, C. M.; Klabunde, K. J.; Hadjipanayis, G. C.; Devlin, E.; Kostikas, A., Size-dependent magnetic properties of MnFe2O4 fine particles synthesized by coprecipitation. Physical Review B 54 (1996) 9288-9296.
35. Kim, Y. I.; Kim, D.; Lee, C. S., Synthesis and characterization of CoFe2O4 magnetic nanoparticles prepared by temperature-controlled coprecipitation method. Physica B: Condensed Matter 337 (2003) 42-51.
36. Arelaro, A. D.; Lima Jr, E.; Rossi, L. M.; Kiyohara, P. K.; Rechenberg, H. R., Ion dependence of magnetic anisotropy in MFe2O4 (MFe, Co, Mn) nanoparticles synthesized by high-temperature reaction. Journal of Magnetism and Magnetic Materials 320 (2008) e335-e338.
37. Carta, D.; Casula, M. F.; Falqui, A.; Loche, D.; Mountjoy, G.; Sangregorio, C.; Corrias, A., A Structural and Magnetic Investigation of the Inversion Degree in Ferrite Nanocrystals MFe2O4 (M = Mn, Co, Ni). The Journal of Physical Chemistry C 113 (2009) 8606-8615.
38. Smit, J.; Wijn, H. P. J., *Ferrites: physical properties of ferrimagnetic oxides in relation to their technical applications*; Philips Research Laboratory, Eindhoven, The Netherlands: Philips Research Laboratory, Eindhoven, The Netherlands, 1959.
39. Morales, M. P.; Veintemillas-Verdaguer, S.; Montero, M. I.; Serna, C. J.; Roig, A.; Casas, L.; Martinez, B.; Sandiumenge, F., Surface and internal spin canting in gamma-Fe2O3 nanoparticles. Chemistry of Materials 11 (1999) 3058-3064.
40. Crespo, P.; de la Presa, P.; Marin, P.; Multigner, M.; Alonso, J. M.; Rivero, G.; Yndurain, F.; Gonzalez-Calbet, J. M.; Hernando, A., Magnetism in nanoparticles: tuning properties with coatings. Journal of Physics-Condensed Matter 25 (2013) 21.
41. Hergt, R.; Dutz, S.; Muller, R.; Zeisberger, M., Magnetic particle hyperthermia: nanoparticle magnetism and materials development for cancer therapy. Journal of Physics-Condensed Matter 18 (2006) S2919-S2934.

42. Glockl, G.; Hergt, R.; Zeisberger, M.; Dutz, S.; Nagel, S.; Weitschies, W., The effect of field parameters, nanoparticle properties and immobilization on the specific heating power in magnetic particle hyperthermia. Journal of Physics-Condensed Matter 18 (2006) S2935-S2949.
43. Carrey, J.; Mehdaoui, B.; Respaud, M., Simple models for dynamic hysteresis loop calculations of magnetic single-domain nanoparticles: Application to magnetic hyperthermia optimization. J. Appl. Phys. 109 (2011) 083921.
44. Obviously, all particles with smaller SAR values will also contribute to the heating; we just define here a limit for those with the highest heating efficiency.
45. Araújo-Neto, R. P.; Silva-Freitas, E. L.; Carvalho, J. F.; Pontes, T. R. F.; Silva, K. L.; Damasceno, I. H. M.; Egito, E. S. T.; Dantas, A. L.; Morales, M. A.; Carriço, A. S., Monodisperse sodium oleate coated magnetite high susceptibility nanoparticles for hyperthermia applications. Journal of Magnetism and Magnetic Materials 364 (2014) 72-79.
46. Boskovic, M.; Goya, G. F.; Vranjes-Djuric, S.; Jovic, N.; Jancar, B.; Antic, B., Influence of size distribution and field amplitude on specific loss power. J. Appl. Phys. 117 (2015) 103903.
47. Kallumadil, M.; Tada, M.; Nakagawa, T.; Abe, M.; Southern, P.; Pankhurst, Q. A., Suitability of commercial colloids for magnetic hyperthermia. Journal of Magnetism and Magnetic Materials 321 (2009) 1509-1513.